Microchimica Acta (2021) 188: 144
https://doi.org/10.1007/s00604-021-04794-1

ORIGINAL PAPER

Molecularly imprinted polymer amalgamation on narrow-gapped Archimedean-spiral interdigitated electrodes: resistance to electrolyte fouling in acidic medium

Hemavathi Krishnan[1] · Subash C. B. Gopinath[1,2] · M. K. Md. Arshad[1,3] · Hanna Ilyani Zulhaimi[2] · Santheraleka Ramanathan[1]

Received: 25 December 2020 / Accepted: 18 March 2021 / Published online: 31 March 2021

Abstract

A conventional photolithography technique was used to fabricate three types of Archimedean-spiral interdigitated electrodes (AIDEs) containing concentric interlocking electrodes with different electrode and gap sizes, i.e., 150 μm (D1), 100 μm (D2), and 50 μm (D3). The precision of the fabrication was validated by surface topography using scanning electron microscopy, high power microscopy, 3D-nano profilometry, and atomic force microscopy. These AIDEs were fabricated with a tolerance of ± 6 nm in dimensions. The insignificant current variation at the pico-ampere range for all bare AIDEs further proved the reproducibility of the device. The large gap sized AIDE (D1) is insensitive to acidic medium, whereas D2 and D3 are insensitive to alkali medium. D2 was the best with regard to its electrical characterization. Furthermore, uniformly synthesized molecularly imprinted polymer (MIP) nanoparticles prepared with human blood clotting factor IX and its aptamer were in the size range 140 to 160 nm, attached on the sensing surface and characterized. The average thickness of deposited MIP film was 1.7 μm. EDX data shows the prominent peaks for silicon and aluminum substrates as 61.79 and 22.52%, respectively. The MIP nanoparticles-deposited sensor surface was characterized by applying it in electrolyte solutions, and smooth curves with the current flow were observed at pH lower than 8 and discriminated against alkali media. This study provides a new MIP amalgamated AIDE with nano-gapped fingers enabling analysis of other biomaterials due to its operation in an ideal buffer range.

Keywords pH sensor · Aluminum electrodes · Molecularly imprinted polymer · Current-volt · Dielectrode

Introduction

Nanotechnology-assisted sensors have prompted a huge interest for the advancement of biomedical diagnosis, pharmaceutical, and environmental researches [1]. Particularly, biosensor development has been vastly grown in recent years for its promising advantages over other biodetection methods, mainly for its rapid and real-time analysis, point-of-care detection, and miniaturized lab-on-chip tools that are highly reliable [2–4]. Biosensors must be highly specific, independent of physical parameters such as pH and temperature and should be reusable. Besides, wide range of fouling materials and methods that leads to electrode fouling must be considered in biosensor development. Fouling of electrodes will significantly reduce sensor efficiency and performance by blocking the electron transfer [5]. To expand the effectiveness of biosensors so as to allow reliable measurements, usage of polymer and hydrogel-based materials gains attention as electrochemical interfaces to reduce surface biofouling [6]. A typical biosensor uses real biological compound to detect and respond to the specific analyte [7]. However, real biological materials are sensitive and costly. Molecularly imprinting polymer (MIP) mimics the features of real bioreceptors put an end to this hitch in recent years [8]. MIP is a tailor made bioreceptor that has highly cross-linked rigid structure. It is instrically

✉ Subash C. B. Gopinath
subash@unimap.edu.my

[1] Institute of Nano Electronic Engineering, Universiti Malaysia Perlis (UniMAP), 01000 Kangar, Perlis, Malaysia

[2] Faculty of Chemical Engineering Technology, Universiti Malaysia Perlis (UniMAP), 02600 Arau, Perlis, Malaysia

[3] Faculty of Electronic Engineering Technology, Universiti Malaysia Perlis (UniMAP), 02600 Arau, Perlis, Malaysia

stable and capable against extreme environments such as, acid-base, temperature, and organic solvents.

In order to improve the performance of biosensors, two main elements must be considered, i.e., sensing material (receptor), which selectively binds target analyte and transducer, that can transform the binding measures into a readable signal output to reflect the analyte concentration in the test sample [2]. In this study, those two elements were given important for designing and developing an authentic nanobiosensor, where MIP was used as synthetic bioreceptor and interdigitated electrode (IDE) as transducer. IDE is one of the most popular transducers, broadly used in various applications due to their low-cost, simple fabrication process and excellent sensitivity [9]. To rationally design and fabricate an absolute IDE sensor, type of substrate, electrode, and the electrode design are the main factors must be considered for easy to functionalize with various types of receptor. As explained in [10], the thickness of the electrode and its gap are essential parts in the flow of electric. Since the gaps between electrodes are the sensing region, it has been fabricated at micro or nanoscale to be a transducer results in large surface-to-volume ratio of sensing area [11].

Archimedean-spiral IDE (AIDE)

"The spiral and concentric sensors described in this paper have Archimedean spiral structure. Alex-Amor and his team [12] stated that the concentric annular electrode has the property of maintaining constant impedance. Compared to the parallel IDEs, the interaction area to the sensor surface area ratio of AIDE is substantially larger. Albeit, the spiral configuration sturdily constraints the sensing region within 2-mm diameter, which impedes gate-controlled response [13]. The current flow resulting from gap of the circular fingers is relatively small compared to the current flow resulting from the parallel IDE sensor. Therefore, merely a very low operational voltage is required compared to the parallel IDE, and the resulting capacitance is less sensitive to the substance analyzed. Sharp edges in parallel IDEs may cause a sudden current loss due to the strong dielectric flux. In AIDEs, such loss is minimized as arc-shaped electrode finger of the concentric sensors interacts with its neighboring, oppositely charged fingers yields evenly current distribution [14]."

In this paper, the insensitivity of the AIDEs towards pH variations for biomedical applications was analyzed. This is to ensure the acid or alkaline charges in the bioreaction media are not influencing the electrical potentials. In order to enhance the sensitivity of AIDE, an advancement of their selectivity is required so that a particular biodetection can be achieved and assayed [15]. The selectivity of the receptors must be improved to give a steady signal output. The current study utilizes these strategies by amalgamating MIP on the sensing surface of AIDE and evaluated the surface sensitivity/insensitivity to acidic and alkali media containing different ranges of electrolytes.

Experimental

Reagents and materials

P-type silicon wafer as a substrate for the conventional photolithography was purchased from Mallinckrodt Baker (Phillipsburg, USA). Positive photoresist (PR + 1–2000 A) and resist developer (RD6) were acquired from Futurrex, Inc. (NJ, USA). Aluminum (Al) coil for Al deposition and Al etch solutions were obtained from Sigma Aldrich (Missouri, USA). Methacrylic acid (MAA) was purchased from Sangon Biotech (Shanghai, China). Ethylene glycol dimethacrylate (EGDMA) and 2,2′-Azobis(isobutyronitrile) (AIBN) were obtained from Merck Schuchardt OHG (Hohenbrunn, Germany). Sensor surface modification chemicals, (3-Aminopropyl) triethoxysilane (APTES), 1-Ethyl-3-(3-dimethylaminopropyl)-carbodiimide (EDC, 98%), N-hydroxysuccinimide (NHS, 98%), Ferricyanide $[Fe(CN)_6]^{3-}$, Ferrocyanide $[Fe(CN)_6]^{4-}$ and phosphate-buffered saline (PBS, pH 7.4) were procured from Sigma Aldrich (Missouri, USA). All the analytical reagents and solvents were purchased from Sigma Aldrich (Missouri, USA).

Design and development of AIDE

AIDE biosensor was designed using AutoCAD© software with gap spacing of 150 (D1), 100 (D1) and 50 μm (D3) width in between interlocking electrodes and printed on a chrome glass surface as a photomask. The fabrication steps for AIDE consist of cleaning, oxidation, and conventional photolithography processes as shown in Fig. 1a. Initially, p-type silicon wafer was rinsed by piranha solution (3:1 of H_2SO_4 and H_2O_2) and washed with distilled water. Next, a wet oxidation process was performed thermally at 500 °C to build 40-nm oxide layer on the surface of silicon substrate [10]. Then, aluminum metal was deposited through a thermal evaporation process. The standard photolithography technique was started with a photoresist coating. In this process, positive photoresist was coated on the aluminum surface using a spin coating method at 2500 rpm and soft baked at 90 °C for 1 min to remove the moistness and standing wave on the surface. Then, the pattern was transferred to the photoresist surface by UV-exposure for 10 s. The pattern was developed next by dipping a few times in photoresist developer. It was conducted carefully and thoroughly to remove the unexposed Al layer to ease the etching process. Afterwards, the electrode were hard baked at 110 °C for 1 min to eliminate moist and to improve the adhesion among Al and SiO_2 layers. The

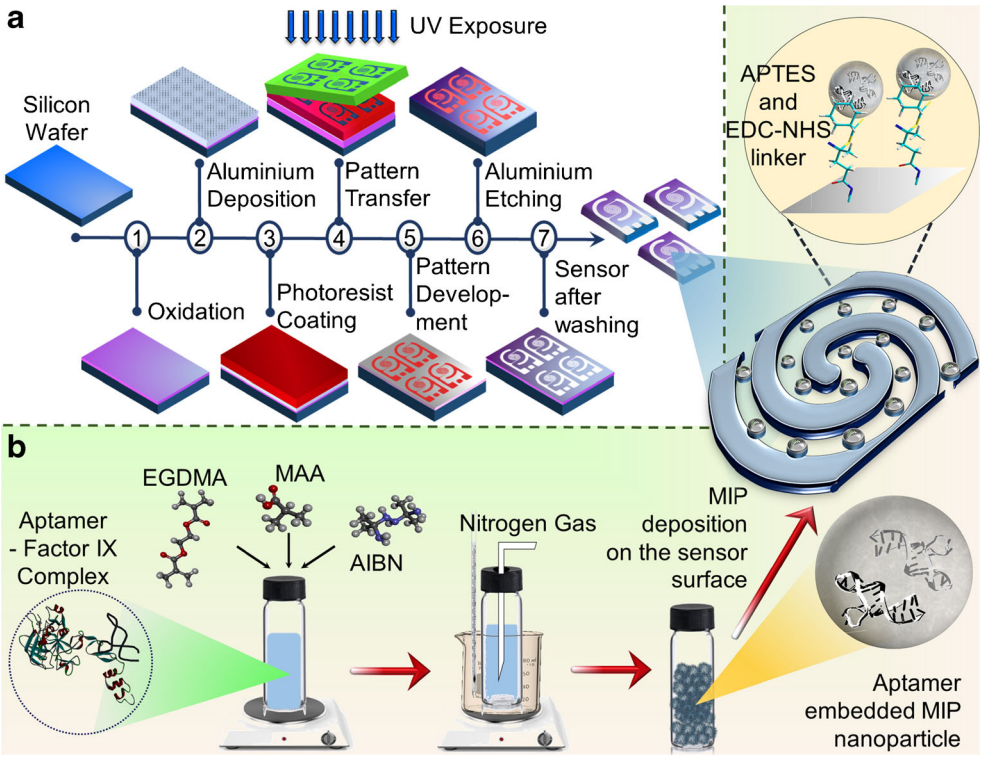

Fig. 1 Schematic illustration of overall research. **a** A process of conventional photolithography technique for AIDE fabrication. **b** Graphical presentation of MIP. Synthesized by precipitation polymerization and immobilization of MIP nanoparticles on AIDE sensor using APTES/EDC-NHS linker

electrode was subsequently immersed in Al etching solution until eluting the unwanted area completely [11]. Finally, the devices were washed with acetone, followed by distilled water and dried under the blower. The devices were kept in dry cabinet to avoid formation of oxidation layers which could upshot electrical properties.

Surface characterization of AIDE

The fabricated AIDEs were characterized by scanning electron microscope (SEM, Hitachi, S-4300 SE, Japan), high power microscope (HPM), 3D-nanoprofilometry (Hawk 3D Optical-Surface Profiler, South Korea), and atomic force microscope (AFM: SPA400-SPI4000, Japan) to authenticate the accuracy of fabricated AIDE surface.

Screening devices by electrolyte scouting

The buffer solutions from pH 2 to 12 were tested on three (3) types of AIDE fabricated surface to evaluate the sensitivity of the sensor to the eletcrolytes. The sensor was placed on the probe station. The positive and negative probe needles were set properly on the electrode pads. The current variation of the device was measured using Picoammeter voltage/current supply (Keithley 6487). Then, 2 μL of pH 2 solution was dropped on the circular surface of device 1. Measurements were by a dual-probe station with the current-volt supply from 0 to 2 V at the sweeping intervals of 0.1 V, generated by the ammeter. The output signal produced by the device was measured. Next, 2 μL of pH 3 solution dropped on the surface following the washing process. The method were repeated until pH 12 and the current variations were recorded. Each interval was washed with distilled water to avoid conjoin effect from previous electrolytes. Unless otherwise stated, all experiments were performed at room temperature and wet condition has been maintained. Ten volumes of 10 mM PBS (pH 7.4) was used to wash the surface in between each immobilization/interaction. All the modifications on the sensor surface has been performed as a continuous way.

MIP synthesis and deposition

MIP was synthesized by radical initiated aqueous precipitation polymerization using aptamer-human blood clotting factor IX protein complex (Apta-FIX) as template. MAA, the functional monomer was mixed with Apta-FIX in acetonitrile-toluene (7:3 v/v) to form a pre-polymerized complex. The mixture was then further added with EGDMA-AIBN mixed solution, which was pre-heated at 60 °C to initiate the polymerization. The ratio of template for functional monomer to cross-link is 1:4:20. The mixture was purged with nitrogen gas and closed the lit tightly for 24-h polymerization at 40 °C oil bath. The polymers then collected and rinsed with 5% SDS and 5% acetic acid in methanol to eliminate the protein impurities, which yield cavities that are complementary to the factor IX protein. Next, the solvent elements entrapped in polymers were washed with distilled water. The eluted solvents were examined by UV-vis spectroscopy to

monitor the template removal. Finally, the polymers were dried in vacuum oven for 24 h. The MIP now is capable to capture or fill the hollow space that formed during washing process.

After screening the best bare device from pH scouting, MIP was deposited on the sensor to functionalize the sensing surface. To remove the impurities on the sensing surface, AIDE was initially rinsed with 30% ethanol. Then, 2% APTES was loaded on the active surface of AIDE to construct the amine-group on the sensing surface. After incubation at ambient temperature for 1 h, the sensor was washed by ethanol and distilled water. MIP particles were modified with EDC-NHS prior to deposition. Then, 2 μL of modified MIP solution was dropped on the sensing area and incubated for 1 h. Finally, the sensor was rinsed with distilled water and dried under nitrogen gas. The overall MIP synthesis process is illustrated in Fig. 1b.

Electrical and electrochemical characterization

For electrical characterization, the similar pH scouting analysis as written above was performed with MIP-deposited device using Keithley picoammeter. The electrochemical characterization was studied by electron impedance spectroscopy. The impedance spectrum was measured on MIP-deposited device at an open circuit potential in the frequency range of 1 MHz to 0.02 Hz, with a 100 mV amplitude. The sensor has been characterized by dielectric measurement for pH 3 to 10 using 2 mM $[Fe(CN)6]^{4-/3-}$ redox buffer that mixed with pH buffer in equal quantity. All the measurements were carried out at room temperature.

Results and discussion

The research covers development of AIDE, visual, and electrical characterization to enrich electrolyte non-fouling. Besides, human blood clotting factor IX imprinted polymers (MIPs) were overlaid on fabricated AIDE. The MIP-AIDE electrical properties were investigated by pH scouting.

Surface characterization of AIDE

Surface characterization was done for visualizing the peripheries and differences in finger as well as gap sizes of the fabricated AIDE in comparison with the designed dimension. For easy understanding, three (3) different gap sized sensors were abbreviated as D1, D2, and D3 for 150, 100, and 50 μm, respectively. Figure 2a illustrates the core design and dimension of the AIDE sensor. Only the gap and electrode widths were manipulated for D1, D2, and D3. The total area of spiral electrodes was about 3.14 μm^2, defined as the sensing area. The SEM images of fabricated AIDE are shown in Fig. 2b–d. It is clearly indicated by projecting obvious differences among them in terms of the gap and electrode finger sizes. The images affirm the accuracy of the fabricated device using photolithography technique, where the gap and electrode widths are with only ± 6 nm of variations. Conversely, the radius gap in between two finger edges at the center point is maintained at 100 μm for all three devices to obtain an Archimedean-spiral and for the stable distribution of current frequency during analysis.

The surface topography was analyzed by 3D-nanoprofiler as shown in Fig. 2e. The clean and smooth surfaces for each layer verifying the device is free from impurities, which attested the perfect fabrication was handled. The silicon surface and the Al electrode surface are seen prominently by the color variation for each layer. Blue color denotes the silicon surface and orange color denotes the Al electrode. More images of 3D-profiler can be found in supplementary information (Fig. S1 c-d, Fig. S2 c-d, Fig. S3 c-d and the corresponding optical images in Fig. S1 e, Fig. S2 e and Fig. S3 e). All three devices are showing the same color variations for each layer confirm the height of layers are approximately same. The average height of Al electrode from the base level is 71.2 μm. For all three devices, minimum height of ~ 4.25 μm from the base level and maximum height of ~ 90.7 μm were observed.

Figure 2f–h show the images under HPM for each devices. The facet of D1 under HPM with 150 μm gap space was shown in Fig. S1 b from another perspective. HPM images of D2 and D3 are included in supplementary information as Fig. S2 b and Fig. S3 b. Overall, an immaculate and neat surface of the device with the gap and finger width are clearly witnessed under HPM. The surface characterization using HPM revealed the finger gap sizes as such 155 μm, 98 μm, and 46 μm for D1, D2, and D3, respectively. The variation of peripheral dimension from the original design was about 6 μm. Therefore, it is concluded that the etching was attained entirely, and the outcome product is well-matched with the photomask pattern. AFM analysis was done on the edge of the finger (Fig. 2i) to visualize 3D image. It is displaying apparent difference of the Al electrode and platform of silicon oxide surface by distinctive height and morphology of each layer.

Electrical characterization: performance of AIDE

Before performing pH sensitivity analysis, the reproducibility of three (3) fabricated device was studied based on current generated on the bare devices, also known as amperometry measurement. Figure 3a infers the reproducibility chart of the bare devices with three different finger gap sizes. The current to voltage (I–V) measurement was conducted to observe the

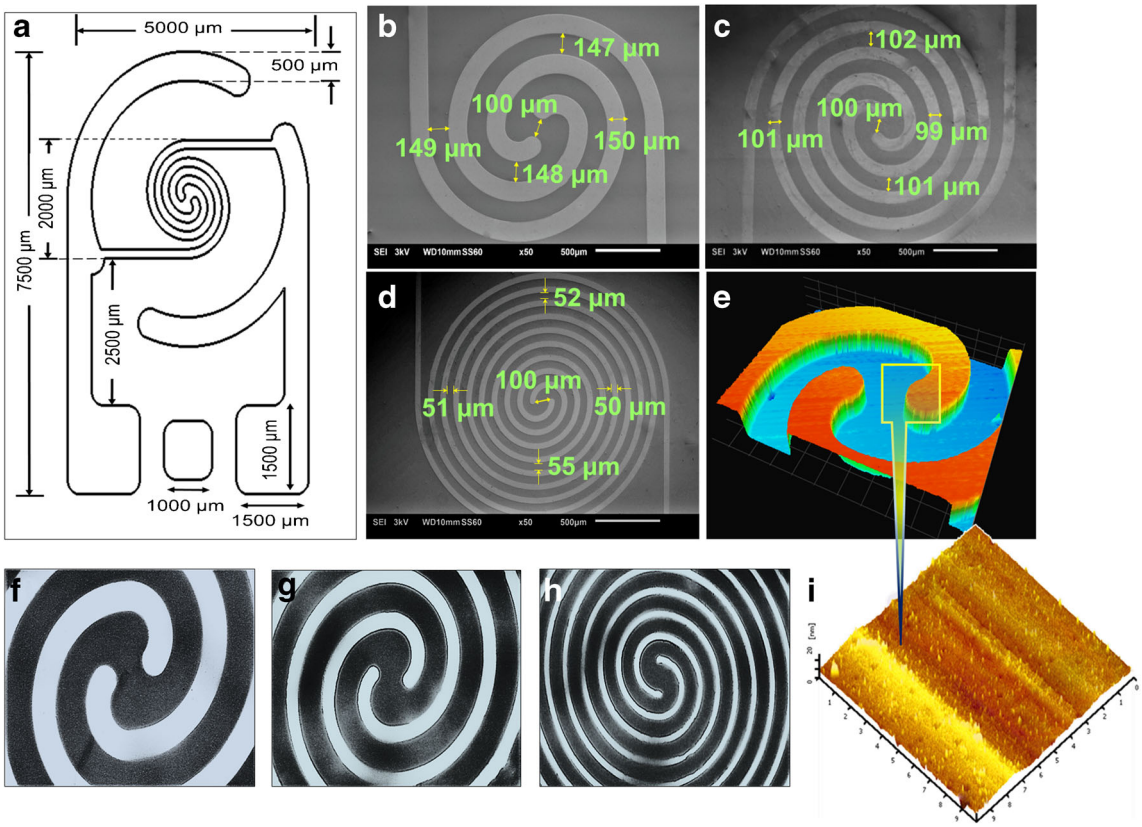

Fig. 2 Surface characterization. **a** Core design of Archimedean-spiral IDE. It was imprinted on 3 devices with different gap sizes. **b–d** Show the electrode and gaps of device 1, 2, and 3 and their corresponding measurement obtained under SEM. **e** 3D image obtained under 3D-nanoprofiler. **f–h** HPM images of fabricated devices with different gap sizes. **i** Depicting the center edge of the sensing area

dielectric changes at bare condition for the supplied voltage from − 2 to 2 V. For all three devices, the current response at the starting point varied but at the end, it has reached slightly similar current values. All the devices were attained nearly zero (0) current at − 1 V supply. Throughout I–V measurements until 2 V, the current ranges were shown to have parallel variations from − 1 V. The maximum current value reached for D1, D2, and D3 are 1.5E-10 A, 2.2E-10 A, and 3.0E-10 A, respectively. The differences are in pico ampere range. Since it is negligible, it is concluded that the devices are well fabricated and reliable to use without any circuit shortages.

Electrical characterization: electrolyte scouting

Photographs of pico-ammeter probe station and fabricated device are as shown in inset Fig. 3a. The fabricated devices were electrically validated by studying the current response at different electrolytes. All three devices were tested from pH 2 to 12 to select the best device with non-resistant electrolytes. Corresponding current variation from hydrogen ions (H^+) and hydroxyl ions (OH^-) movements of pH solutions was recorded and charted in Fig. 3b–d. D1 (Fig. 3b) showing prominent response for pH 12 followed by pH 11, 10, and 9. The maximum current amplified was 2.5E-5 A at pH 12. On the other hand, lower current was attained from pH 2 to 8 as displayed in figure inset. Based on the current responses, D1 is suitable for buffer medium below pH 8. Conversely, D2 (Fig. 3c) showing noticeable current response for pH 2, pH 3, and pH 12. As observed in figure inset, D2 is suitable for medium with alkaline pH ranges as very low current amplified. Figure 3d shows the current response for D3 with smallest finger gap size. It implies its suitability for alkali solution similar to D2. Both D2 and D3 exhibiting apparent response for acidic medium with maximum current amplification of 1.1E-3 and 3.0E-4 A, respectively. Contrariwise, insignificant current response from pH 4 to 11 for D2 and pH 4 to 12 for D3 as depicted in their respective figure inset revealed insensitivity towards neutral and alkali medium. Although, D2 and D3 are insensitive for neutral and alkali medium, D2 showing least fluctuation of current response at different pH levels. For the application of bio-analysis, it is crucial to eliminate high acidic and high alkali medium sensitive device. Thence, D2 shows insensitivity for mild acidic and mild alkali

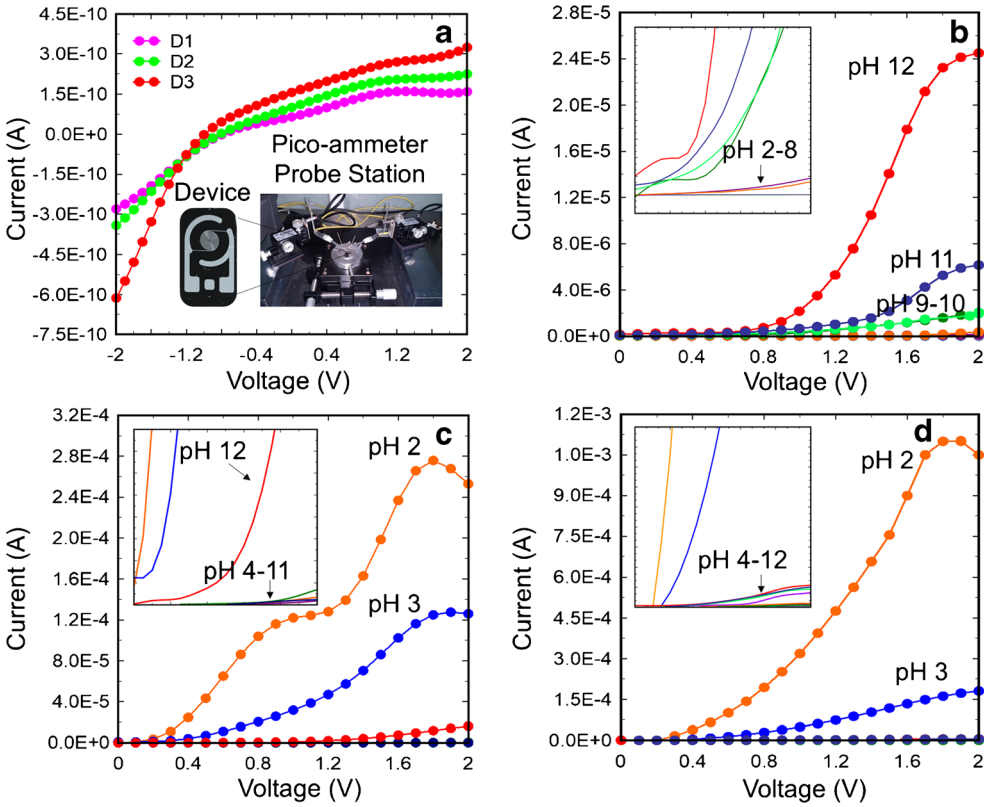

Fig. 3 Electrolyte scouting: device performances. **a** Reproducibility graph is shown for D1, D2, and D3. Pico-ammeter setup and fabricated device photographs are enclosed as figure inset. Electrical potentials were generated by three different gap sized devices at their bare condition to assess the similarity of current amplified. **b**–**d** Current generation by D1, D2, and D3. Responses of pH concentrations were noticed. The figure inset shows an enlarged view of low current amplification

solution. The dissociation of ions from highly acidic and alkaline media amplifies the current due to the highest mobility of electrons transfer.

When pH solution is introduced, a charge distribution and corresponding potential occur at the interface of electrode until both phases attain equilibrium. The gap size of D1 is substantially larger than D2 and D3, which creates more spaces for ionic flux and charge distribution which facilitates rapid movement of counterions towards the electrode interface. Variance pH responses for D1 compared to D2 and D3 occurred due to the unequal amount of charged ions and the space for charge distribution. As the gap size decreases for D2 and D3, the concentration of H^+ ions from acidic medium creates more charge capacitance on silicon surface and consequently higher current amplification of the sensor attained. Another phenomenon for this occurrence is the conductivities of the pH solutions used. The conductivity range of buffer solution increases with the change in H^+ concentration. D2 and D3 is very responsive to pH 2 and 3, presumably because the conductance is higher, resulting accelerated current response [16].

In addition, AIDE dimension also influences the electrolyte sensitivity. It is perceived that smaller the gap, higher the current response. The results again elucidate the flux of ions in varied electrolytes. A rapid ionic mobility in smaller gapped devices elevates the conductivity and current response. The more electrode fingers decreases the impedance and thus capacitance will be higher which yields very responsive current amplification. Therefore, D2 with finger gap size of 100 μm was selected as the best device for further experiment. Choosing D2 is an added advantage for its pattern. The moderate gap size between electrode fingers is ample enough to provide stable current response without false positive reading.

MIP characterization

Molecular imprinting is a creation of artificial selective binding sites with the memory of template molecule [17]. MIP nanoparticles were successfully synthesized by the aqueous precipitation polymerization. Apta-FIX complex was prepared separately in phosphate buffered saline (PBS) solution as template complex while MAA was pre-dissolved in acetonitrile-toluene (7:3 v/v). In pre-polymerization stage, these solutions were mixed to allow functional monomers stoichiometrically interact with template complex, in homogenous organic phase. The possibility of protein precipitation from acetonitrile is reduced by mixing with aprotic toluene solution. Mixture of polar acetonitrile and non-polar toluene acts as porogenic solvent to produce the MIP nanoparticles with broad distribution of pores. This ensures the protein to become permeable into the polymer matrix and reach the cavities in rebinding phase [18]. Additionally, these porogenic solvents facilitate strong polar interactions such as electrostatic interactions and hydrogen

bonds between template complex, monomers, and the cross-linkers [19, 20].

To evidence the protein removal from MIP nanoparticles, UV-vis spectrophotometry analysis was employed. The result is shown in Fig. 4a. An absorbance peak was observed at 280 nm from the factor IX stock in PBS buffer [Fig. 4a. (i)]. With the baseline of washing solvent (5% SDS and 5% acetic acid), an apparent absorbance attained in the initial protein removal stage [Fig. 4a. (ii)]. After several washes, the absorbance reduced from 0.55 to 0.09 O.D. at last [Fig. 4a. (iii)], attests the efficient and complete elution of the protein impurities. Figure 4a. (iv) is the absorbance from methanol wash which eliminates other redundant materials. Absorbance reduction at 280 nm in final wash and methanol wash confirms that, there is no more protein fragments entrapped in the MIP nanoparticles.

MIP nanoparticles were characterized under SEM to obtain particle size and porosity distribution as shown in Fig. 4b, c. It displays the MIP nanoparticles at 10000 times of 1 μm scale and 30,000 times of 0.5 μm. Both images are showing clear picture of aggregated spherical particles. Using imageJ software, the uniform distribution of particle size was analyzed and displayed as histogram in Fig. 4d. About 85% of the particles are in the range of 140 to 160 nm. Figure 4 e shows diffractograms of MIP nanoparticles from X-ray diffraction (XRD) analysis, in the scan range 20-to-80° angle. Only two broad peaks observed at 29° and 40° imply the polymer is amorphous material, and the crystallinity was not deteriorated during template removal stage and drying stage. No sharp diffraction describes MIPs are homogeneous nature. This is basically consistent with the earlier works [21, 22]. The figure inset of Fig. 4e showing the photographs of MIP nanoparticles in gel form before template removal process and the final product of MIP nanoparticles.

Functionalization of AIDE by MIP for target printing

Based on pH scouting analysis, device 2 with 100 μm gap (D2) was modified with APTES to form self-assembled monolayer of alkoxysilane. APTES generally has been used in biosensing platform for its advantages of biocompatibility and the excellent affinity. Next, MIP nanoparticles were modified by EDC-NHS solution before deposition to impose monolayer binding on the sensing surface. Basically, EDC is a carbodiimide molecule that activates the carboxyl and forms an amine reactive functional group that immediately reacts

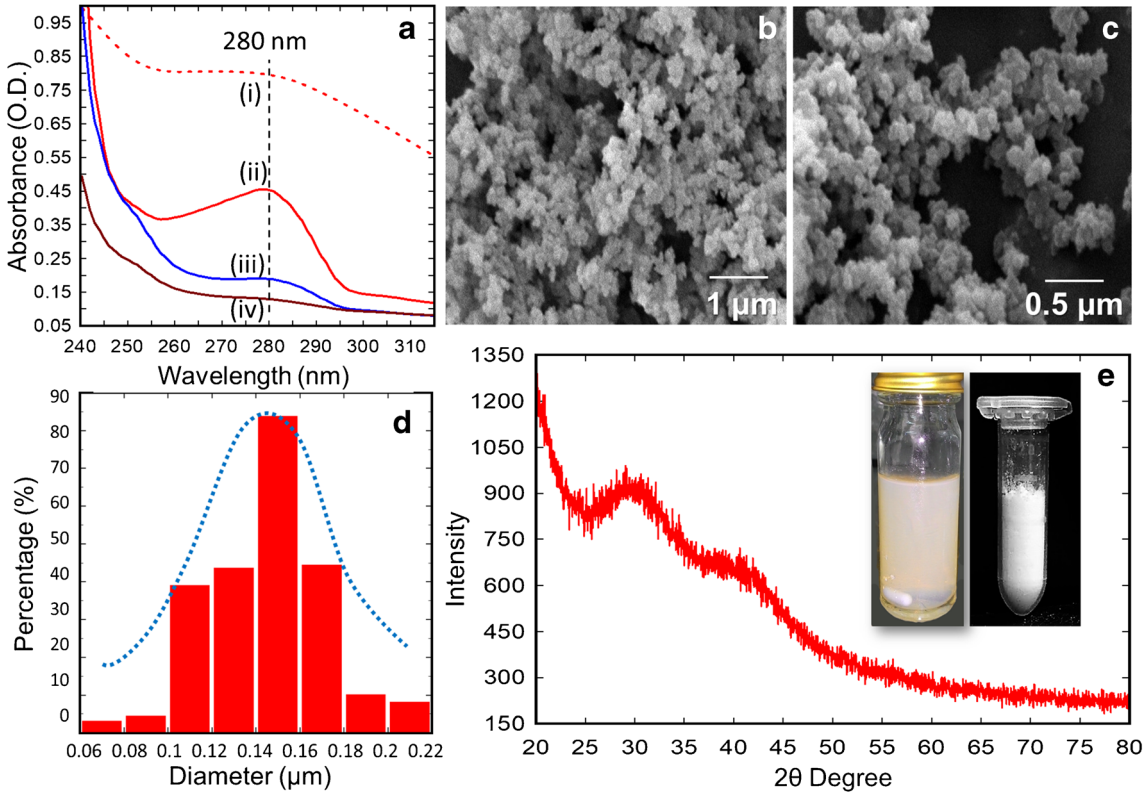

Fig. 4 MIP nanoparticles characterization. **a** UV–vis absorption spectroscopy to monitor the template removal from MIP. **b** 10,000 times magnified SEM image. **c** 30,000 times magnified SEM image. **d** Histogram represents MIP nanoparticles size distribution. **e** Diffractograms of MIP nanoparticles after template removal. Figures inset show the gel form of MIP during synthesis process and final product of MIP nanoparticles

with primary amine to form semi-stable O-acylisourea ester. Since, EGDMA was used as cross-linker to synthesize MIP, the produced nanoparticles are surrounded by the exposed carboxyl (COOH) groups. EDC-NHS deforms its N-H structure and stimulates negatively charged COOH of EGDMA [23]. This unstable O-acylisourea ester has the potential for MIP nanoparticles to covalently conjugate on APTES modified device.

Surface characterization of MIP-AIDE

The surface of MIP-AIDE was characterized by 3D nanoprofiler, Energy dispersive X-ray spectroscopy, and HPM and AFM results are displayed in Fig. 5. Figure 5a is the color variation to indicate the height. The surface of bare device included as reference in Fig. 5b to see the difference between bare and MIP-deposited device. Adhered MIP particles on the device is clearly visible in Fig. 5c, d. For the bare device, the bottom surface color is blue. However, MIP-deposited device is showing a green-yellow shaded bottom surface. This obviously evidences that the MIP nanoparticles were deposited as a uniform layer. The uniformity was further proved by the surface roughness graph in Fig. 5e. The uniform layer of polymer also helps in giving a stable measurement when applying for biosensing. The uneven nanoparticle deposition may affect the current flow due to imbalanced biodetection. According to this graph, minimum height of Al electrode from base level (0.9 μm) and the maximum height of rough surface (2.28 μm) were yielded, and average thickness of deposited MIP film was 1.7 μm. MIP nanoparticles attach on both the electrode and the gaps. MIP nanoparticles attach on the gap through the modification of APTES on SiO_2 surface while carboxylate bridging on aluminum oxide electrode by topotactic reaction [24].

Energy dispersive spectrometer (EDX) peak of MIP deposited sensor is shown in Fig. 5f. EDX data shows the peaks arise prominently for silicon and aluminum substrate as weighed percentage of 61.79 for silicon and 22.52 for Al. Other elements such as carbon, oxygen, and nitrogen also

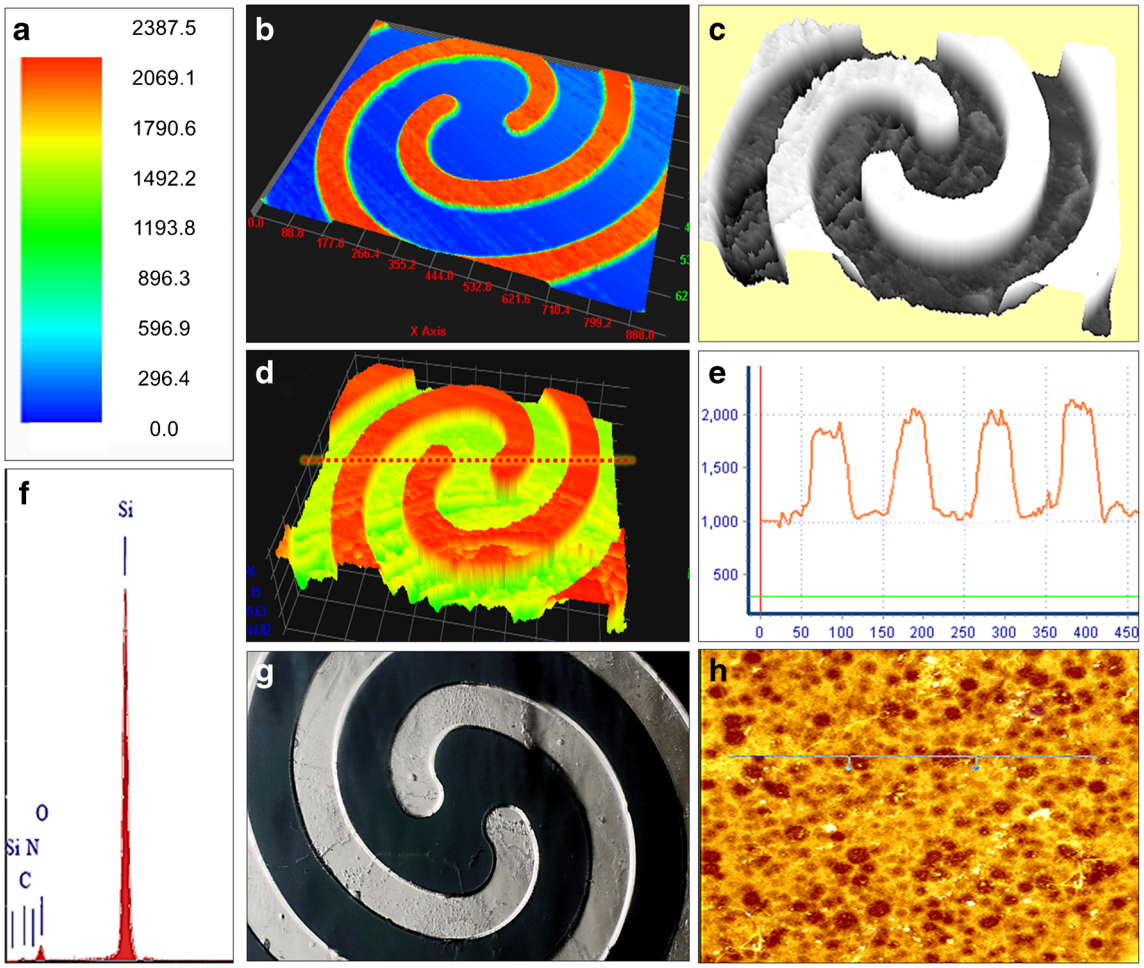

Fig. 5 MIP-AIDE topography. **a** Color variations depict the height from surface platform. **b** Image of bare device obtained from 3D-nano profiler. **c**–**d** Surface texture analysis by 3D-nano profiler. **e** Surface roughness graph corresponding to the image. **f** EDX data of MIP-AIDE. **g** HPM image of MIP-AIDE. **h** 2D image of MIP-deposited AIDE surface obtained from AFM

detected in this analysis evidence the deposition of MIP nanoparticles. MIP deposited surface was further characterized by HPM as presented in Fig. 5g. The boundaries of Al electrode and smooth surface also proving a perfect MIP deposition was achieved without any particles setting. The surface color also changed after MIP deposition comparing with the HPM image of bare device (Fig. 2g).

Electrical characterization of MIP-AIDE

MIP-deposited device was characterized by electrolyte sensitivity analysis similar to the above method. The current distribution pattern and the ion transferring mechanism of AIDE are explained in Fig. 6a. When the voltage applied, a dielectric surface formed in between electrode causing a dipole moment. When electrolytic solution introduced, potential difference occurs in the dipole area causing the ions move through the solution due to the electric field. The negatively charged ions headed for the anode and positively charged ions headed for the cathode as shown in the inset figure. The ions are neutralized at the electrode surface and the electrons transfer over the circuit. The dipole electric field pattern changes corresponding to the electron transfers which produces variation in current readout.

Figure 6b shows the electrolyte response on MIP-AIDE. MIP-AIDE is very unresponsive below pH 8. Only slight current variation was attained as the pH increases from pH 2 to 8. An outstanding current response was observed beyond pH 9 and pH 2. Ideally, pH 2 contains more H^+ ions whereas pH 9 and above contains more OH^- ions. As illustrated in Fig. 6c, d, when introducing high acidic and alkaline solutions on the sensor surface, the ion density increases, which fluctuating dielectric properties and affects the electric field patterns in between the cathode and anode electrode. Another possible reason might be the swelling of MIP nanoparticles at high acidic and alkali medium which causes ionic polarization and raised the current response. At this state, the surrounding EGDMA crosslinker of MIP nanoparticles become partially charged [25]. When high ionic electrolytes introduced, rapid mobility of ions in sensing area produces greater current output. This limits the sensor compatibility for electrolytes with lower or higher pKa values.

However, the MIP nanoparticles mainly synthesized for protein detection where most of the biomolecules are neutral nature. Therefore, the pH scouting outcome of MIP deposited sensor is convincingly reliable as responding very lower current variation near neutral pH. Compared to bare device electrolyte analysis, MIP amalgamated AIDE shows lower and smooth current response below pH 8. This shows that MIP-AIDE works with high stability. It is concluded that, this device can be used for other bioanalysis applications. Considering lifetime, storage of the bare sensing surface was possible for several months when stored under a proper

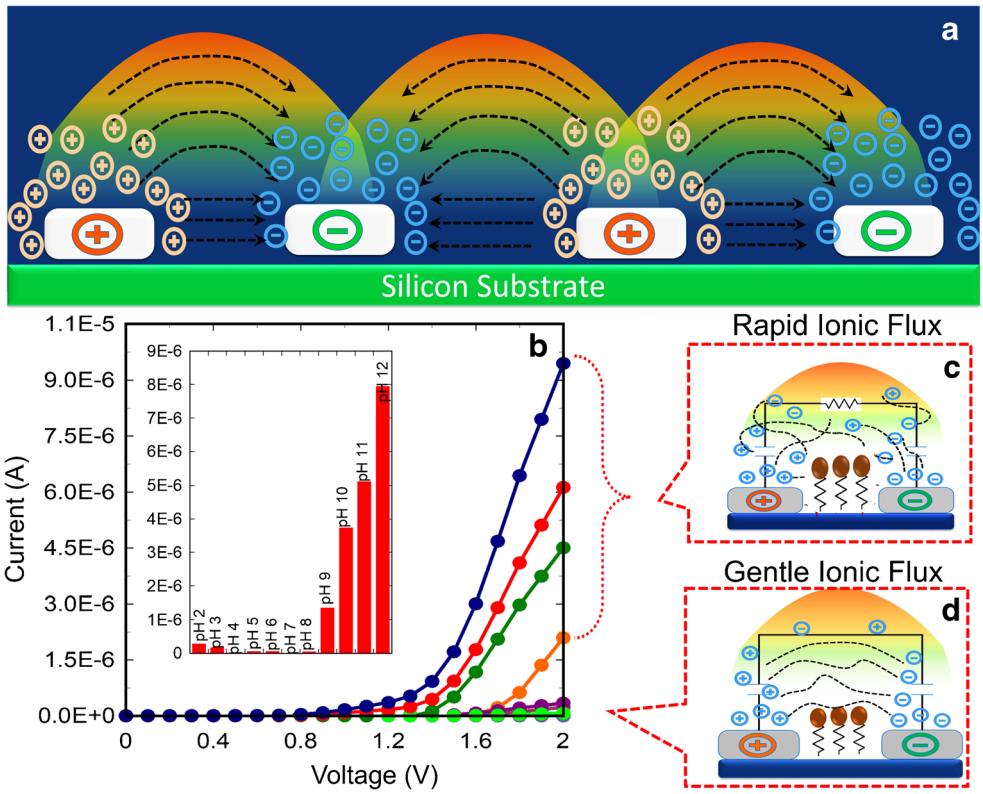

Fig. 6 Electrolyte scouting on MIP-AIDE. **a** Illustration of electric field pattern produced when voltage applied to AIDE. **b** Sensitivity of MIP deposited AIDE towards pH variations. Figure inset shows current response of MIP-AIDE sensor at 2 V towards various electrolytes. **c**–**d** Electric field pattern changes at gentle and rapid ionic flux

condition using the desiccator. With the same device upon attaching MIP, the surface stability was noticed to be lost by ~ 10% after a month.

Electrochemical characterization of MIP-AIDE

AIDE works as capacitance or impedance sensor based on faradaic or non-faradaic way [26]. The electrochemical study was done by impedimetric measurement in faradaic electron impedance spectroscopy (EIS) for pH 3 to 10 buffer solutions with the coupling of $[Fe(CN)_6]^{4-/3-}$ redox solution. The data were evaluated by ZsimpWin software. Figure 7a shows the best fitted Nyquist plot for bare AIDE, MIP-AIDE, and pH 3 to pH 7 with Randles equivalent circuit model. From the fitted data, the charge transfer resistance (Rct) (the right intercept of the semi-circle) is monitored for each pH buffer. The Rct point of Nyquist plot propagates for each increament of pH values. It is observed the electron diffusion also varies for each pH. For pH 7 and 8, there is no diffusive response is observed. Nyquist plot for pH 9–10 is included in supplementary information (Fig. S4.) as the drastic electron diffusion in alkali medium attained due to presence of more negatively charged −OH ions.

Total impedance, Z versus frequency represented by Bode plot of the electrochemical system is illustrated in Fig. 7b. Sweeping voltage frequency from 1 MHz to 0.02 Hz, the MIP-AIDE achieved constant impedance from 1 MHz until 0.2 Hz due to the Archimedean pattern that distributed the current evenly and it proves the stability of the sensor. But then, for frequencies lower than 0.2 Hz, noisy pattern of impedance occurred which could affect the sensor capacitance. This caused by the kinetics of electron movement across the electrode will escalate when there is a low frequency of voltage is applied [27]. Thus, 0.2 Hz to 1 MHz could be the working frequency range for this sensor. The capacitance value for each pH buffer solution was predicted from Zsimpwin software at 1 Hz and plotted as figure inset in Fig. 7b. The capacitance of MIP-AIDE increases with the rise in pH values. The higher concentration of H+ ions in acidic medium increases the charge density and diminishes the electrical fields pattern in the buffer. Subsequently, the dielectric constant of various pH buffers manifests its permittivity and yield changes in the capacitance [28–30].

Conclusion

In this manuscript, Archimedean spiral-shaped IDE was fabricated with Al as conducting electrodes. The AIDE was fabricated for three different finger gap sizes using the conventional photolithography technique and characterized by SEM, HPM, AFM, and 3D-nanoprofiler. Molecularly imprinted nanoparticles were synthesized by embedding aptamer to detect FIX protein and characterized by SEM and XRD. Molecularly imprinted polymer nanoparticles were used as conjugating material on AIDE for the detection of human blood clotting factor IX protein. Electrolyte scouting I–V measurement on bare devices has confirmed the reproducibility of the sensor. Electrical characterization was done for AIDE before and after MIP nanoparticle conjugation. The MIP-AIDE is insensitive below pH 8. To further analyze the insensitivity of MIP-AIDE, electron impedance analysis was done. Both electrical and electrochemical studies confirm that pH 3 to 8 are the ideal buffer pH levels for the fabricated AIDE and the similar sensing surfaces. The Archimedean pattern increases the stability of the sensor by uniform current distribution which is compatible for various nanomaterial coupling or other biomaterial detection. Considering the limitations of this sensor, this study uses the oxide material to attach MIP, whereas other substrates might need a further optimization. Archimedean-spiral interdigitated electrodes have gaps at micrometer and when this gap size is reduced to nanometer it generates the short circuit.

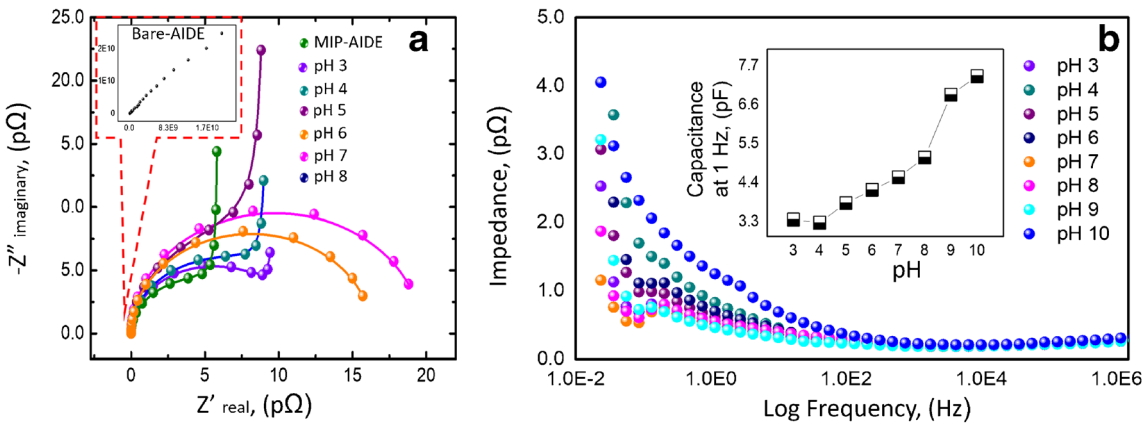

Fig. 7 Electrochemical analysis of MIP-AIDE. **a** -Z″ vs. Z′ Nyquist plot for pH scouting on MIP-AIDE with an inset showing impedance for bare AIDE. **b** The total Z vs. frequency 'Bode plot.' The figure inset is capacitance attained from various pH buffer at 1 Hz

Supplementary Information The online version contains supplementary material available at https://doi.org/10.1007/s00604-021-04794-1.

Funding This work was supported by The Ministry of Education, Malaysia for providing financial support under Fundamental Research Grant Scheme [FRGS/1/2019/TK10/UNIMAP/03/3]. SCBG was supported by a special grant (9001–00596) from Universiti Malaysia Perlis.

Declarations

Conflict of interest The authors declare that they have no competing interests.

References

1. Ramanathan S, Gopinath SCB, Md. Arshad MK, Poopalan P (2019) Multidimensional (0D-3D) nanostructures for lung cancer biomarker analysis: comprehensive assessment on current diagnostics. Biosens Bioelectron 141:111434. https://doi.org/10.1016/j.bios.2019.111434
2. Dalila RN, Md. Arshad MK, Gopinath SCB et al (2019) Current and future envision on developing biosensors aided by 2D molybdenum disulfide (MoS2) productions. Biosens Bioelectron 132:248–264. https://doi.org/10.1016/j.bios.2019.03.005
3. Shrivastava S, Jadon N, Jain R (2016) Next-generation polymer nanocomposite-based electrochemical sensors and biosensors: a review. Trends Anal Chem 82:55–67. https://doi.org/10.1016/j.trac.2016.04.005
4. Ding S, Das SR, Brownlee BJ, Parate K, Davis TM, Stromberg LR, Chan EKL, Katz J, Iverson BD, Claussen JC (2018) CIP2A immunosensor comprised of vertically-aligned carbon nanotube interdigitated electrodes towards point-of-care oral cancer screening. Biosens Bioelectron 117:68–74. https://doi.org/10.1016/j.bios.2018.04.016
5. Rad AO, Azadbakht A (2019) An aptamer embedded in a molecularly imprinted polymer for impedimetric determination of tetracycline. Microchim Acta 186:2–11. https://doi.org/10.1007/s00604-018-3123-9
6. Campuzano S, Pedrero M, Yáñez-Sedeño P, Pingarrón JM (2019) Antifouling (bio)materials for electrochemical (bio)sensing. Int J Mol Sci 20:423. https://doi.org/10.3390/ijms20020423
7. Lakshmipriya T, Gopinath SCB (2018) An introduction to biosensors and biomolecules. In: Nanobiosensors for biomolecular targeting. Elsevier Inc., pp. 1–21
8. Gui R, Jin H, Guo H, Wang Z (2018) Recent advances and future prospects in molecularly imprinted polymers-based electrochemical biosensors. Biosens Bioelectron 100:56–70. https://doi.org/10.1016/j.bios.2017.08.058
9. Lu B, Liu L, Wang J, Chen Y, Li Z, Gopinath SCB, Lakshmipriya T, Huo Z (2020) Detection of microRNA-335-5p on an Interdigitated electrode surface for determination of the severity of abdominal aortic aneurysms. Nanoscale Res Lett 15:105. https://doi.org/10.1186/s11671-020-03331-y
10. Ramanathan S, Gopinath SCB, Md Arshad MK, Poopalan P, Loong FK, Lakshmipriya T, Anbu P (2019) Assorted micro-scale interdigitated aluminium electrode fabrication for insensitive electrolyte evaluation: zeolite nanoparticle-mediated micro- to nano-scaled electrodes. Appl Phys A Mater Sci Process 125:548. https://doi.org/10.1007/s00339-019-2833-0
11. Partel S, Kasemann S, Matylitskaya V, Thanner C, Dincer C, Urban G (2017) A simple fabrication process for disposable interdigitated electrode arrays with nanogaps for lab-on-a-chip applications. Microelectron Eng 173:27–32. https://doi.org/10.1016/j.mee.2017.03.014
12. Alex-Amor A, Palomares-Caballero Á, Fernández-González JM, Padilla P, Marcos D, Sierra-Castañer M, Esteban J (2019) RF energy harvesting system based on an archimedean spiral antenna for low-power sensor applications. Sensors (Switzerland) 19:1318. https://doi.org/10.3390/s19061318
13. Pecqueur S, Lenfant S, Guérin D, Alibart F, Vuillaume D (2017) Concentric-electrode organic electrochemical transistors: case study for selective hydrazine sensing. Sensors 17:570. https://doi.org/10.3390/s17030570
14. Oommen BA, Philip J (2020) Enhanced performance of spiral coplanar inter-digital capacitive structures for sensing applications. Sens Imaging 21:1–18. https://doi.org/10.1007/s11220-020-00324-0
15. Slaughter G (2018) Current advances in biosensor design and fabrication. In: R.A. Meyers (ed) Encyclopedia of analytical chemistry, R.A. Meyer. John Wiley & Sons, Ltd, pp. 1–25
16. Manjakkal L, Djurdjic E, Cvejin K, Kulawik J, Zaraska K, Szwagierczak D (2015) Electrochemical impedance spectroscopic analysis of RuO_2 based thick film pH sensors. Electrochim Acta 168:246–255. https://doi.org/10.1016/j.electacta.2015.04.048
17. Xu J, Merlier F, Avalle B, Vieillard V, Debré P, Haupt K, Tse Sum Bui B (2019) Molecularly imprinted polymer nanoparticles as potential synthetic antibodies for immunoprotection against HIV. ACS Appl Mater Interfaces 11:9824–9831. https://doi.org/10.1021/acsami.8b22732
18. Rachkov A, Minoura N (2001) Towards molecularly imprinted polymers selective to peptides and proteins. The epitope approach. Biochim Biophys Acta Protein Struct Mol Enzymol 1544:255–266. https://doi.org/10.1016/S0167-4838(00)00226-0
19. Nabavi SA, Vladisavljević GT, Eguagie EM, Li B, Georgiadou S, Manović V (2016) Production of spherical mesoporous molecularly imprinted polymer particles containing tunable amine decorated nanocavities with CO2 molecule recognition properties. Chem Eng J 306:214–225. https://doi.org/10.1016/j.cej.2016.07.054
20. Pichon V, Haupt K (2006) Affinity separations on molecularly imprinted polymers with special emphasis on solid-phase extraction. J Liq Chromatogr Relat Technol 29:989–1023. https://doi.org/10.1080/10826070600574739
21. Behbahani M, Barati M, Bojdi MK, Pourali AR, Bagheri A, Tapeh NAG (2013) A nanosized cadmium(II)-imprinted polymer for use in selective trace determination of cadmium in complex matrices. Microchim Acta 30:31–35. https://doi.org/10.1007/s00604-013-1036-1
22. Ahmad S, Ahmad S, Agnihotry SA (2007) Synthesis and characterization of in situ prepared poly (methyl methacrylate) nanocomposites. Bull Mater Sci 30:31–35. https://doi.org/10.1007/s12034-007-0006-9
23. Okan M, Sari E, Duman M (2017) Molecularly imprinted polymer based micromechanical cantilever sensor system for the selective determination of ciprofloxacin. Biosens Bioelectron 88:258–264. https://doi.org/10.1016/j.bios.2016.08.047
24. Barron AR (2014) The interaction of carboxylic acids with aluminium oxides: journeying from a basic understanding of alumina nanoparticles to water treatment for industrial and humanitarian applications. Dalton Trans 43:8127–8143. https://doi.org/10.1039/C4DT00504J
25. Dai J, Fidalgo de Cortalezzi M (2019) Influence of pH, ionic strength and natural organic matter concentration on a MIP-fluorescent sensor for the quantification of DNT in water. Heliyon 5:e01922. https://doi.org/10.1016/j.heliyon.2019.e01922
26. Kremers T, Menzel N, Freitag F, Laaf D, Heine V, Elling L, Schnakenberg U (2020) Electrochemical impedance spectroscopy using interdigitated gold–polypyrrole electrode combination. Phys

Status Solidi Appl Mater Sci 217:1900827. https://doi.org/10.1002/pssa.201900827

27. Brosel-Oliu S, Abramova N, Uria N, Bratov A (2019) Impedimetric transducers based on interdigitated electrode arrays for bacterial detection – a review. Anal Chim Acta 1088:1–19. https://doi.org/10.1016/j.aca.2019.09.026
28. Arefin MS, Bulut Coskun M, Alan T, Redoute JM, Neild A, Rasit Yuce M (2014) A microfabricated fringing field capacitive pH sensor with an integrated readout circuit. Appl Phys Lett 104:1–5. https://doi.org/10.1063/1.4881263
29. Cesewski E, Johnson BN (2020) Electrochemical biosensors for pathogen detection. Biosens Bioelectron 159:91–98. https://doi.org/10.1016/j.bios.2020.112214
30. Dudzinski K, Dawgul M, Pluta KD, Wawro B, Torbicz W, Pijanowska DG (2017) Spiral concentric two electrode sensor fabricated by direct writing for skin impedance measurements. IEEE Sensors J 17:5306–5314. https://doi.org/10.1109/JSEN.2017.2719001